JOURNAL OF AGRICULTURAL AND FOOD CHEMISTRY

Reveal Protein Molecular Structural−Chemical Differences between Two Types of Winterfat (Forage) Seeds with Physiological Differences in Low Temperature Tolerance Using Synchrotron-Based Fourier Transform Infrared Microspectroscopy

P. YU,* R. WANG, AND Y. BAI

College of Agriculture, University of Saskatchewan, 51 Campus Drive, Saskatoon S7N 5A8, Canada

Winterfat (*Kraschenninnikovia lanata*) (forage seed) is a long-lived native shrub with superior forage quality for livestock and wildlife. The objectives of this study were to use advanced synchrotron technology [S-Fourier transform infrared microspectroscopy (FTIR)] as a novel approach to reveal protein molecular structural−chemical differences in terms of protein secondary structures between the two types of winterfat (forage) seeds, which show physiological differences in low-temperature tolerances. This experiment was performed at beamline U10B at the National Synchrotron Light Source (NSLS) in Brookhaven National Laboratory (BNL), U.S. Deptpartment of Energy (NSLS-BNL, New York). The results showed that with the synchrotron analytical technique (S-FTIR), the molecular structural−chemical makeup and characteristics of the winterfat seed tissues could be imaged and revealed. The protein secondary structures differed between the large and the small seed tissues. By using the multicomponent peaks modeling method, the results show that the large seeds contained no significant differences ($P > 0.05$) in percentage of β-sheet (average 37.0%) and α-helix (average 24.1%). However, the large seeds contained a lower ($P < 0.05$) percentage of β-turns (18.1 vs 20.1%) and a lower ($P < 0.05$) ratio of β-turns to α-helices (0.8 vs 0.9) and β-turns to β-sheets (0.5 vs 0.6). Our results demonstrate the potential of highly spatially resolved synchrotron-based FTIR microspectroscopy to reveal differences of structural molecular chemistry and protein secondary structures, which are associated with seed size variation and may affect germination behaviors.

KEYWORDS: Synchrotron; FTIR microspectroscopy; molecular chemistry; protein secondary structure; chemical imaging; forage seed tissue; germination behaviors; winterfat

INTRODUCTION

Winterfat (*Kraschenninnikovia lanata*) (forage seed) is a long-lived native shrub with superior forage quality for livestock and wildlife, playing an important role in the ecology of the mixed prairie of North America (*1*, *2*). Larger seeds of winterfat germinate faster and in a higher percentage than smaller seeds, especially at lower temperatures (*3*, *4*). Early-emerging winterfat seedlings have a greater growth rate and a better survival rate than late-emerging plants (*3*), and relatively heavier seeds are desirable for their restoration.

Seed size variation within a seed population is correlated, in many species, with seed vigor (*5*, *6*), seedling recruitment (*7*, *8*), and plant size and the probability of survival (*3*, *9*, *10*). Physiological differences in the low-temperature tolerance between the large and the small seeds of winterfat are associated with the content of soluble cryoprotective sugars and membrane integrity (*11*). However, it remains unknown what the difference is between two seed size classes in their functional biochemical components and structural molecular chemistry, such as protein inherent structure or protein matrix and starch granules associated with protein matrix in dry seeds. These may be associated with higher germination vigor and cold tolerance in large seeds. Some studies show that the irreversible change in protein secondary structures was associated with seed tolerance to desiccation in *Quercus alba* L. (*12*).

Synchrotron-based Fourier transform infrared microspectroscopy (S-FTIR) has been developed as a rapid and direct bioanalytical technique (*13*, *16*). In contrast to traditional "wet" chemical methods, which during processing for analysis often result in destruction of the intrinsic structures of seeds, this technique (*17*), taking advantage of synchrotron light brightness (one million times brighter than sunlight), is capable of exploring the molecular chemistry within microstructures of biological tissues. This technique is able to determine the tissue-localized chemical microstructure without the destruction of inherent

* To whom correspondence should be addressed. Tel: +1 306 966 4132. Fax: +1 306 966 4151. E-mail: yupe@sask.usask.ca.

10.1021/jf051748+ CCC: $30.25
Published on Web 11/04/2005

structures at ultraspatial resolutions (3−10 μm) within cellular and subcellular dimensions (*13*, *16*, *18*, *19*). To date, there has been very little application of this advanced technique (S-FTIR) for the study of seed tissue in relation to seed size variation.

The objectives of this study were to use the synchrotron technology (S-FTIR) as a novel approach to reveal protein molecular structural−chemical differences in terms of protein secondary structure between the two types of winterfat (forage) seeds, which have physiological differences in low-temperature tolerances. Information from the study by the infrared probing of seed inherent structures may be valuable as a guide to relating seed size variation, and thereafter, germination variation in a seed population.

MATERIALS AND METHODS

Winterfat Seeds. Winterfat seeds (diaspores), collection #63, were purchased from Wind River Seed (Manderson, WY), originating from Utah. The diaspores were cleaned by rubbing, fanning, and passing seeds through serial sieves and blowers. Cleaned seeds were separated into two classes using a seed blower based on seed mass and hereafter were referred as seed size classes large and small. The seed weight was significantly different, and the seed moisture content was similar between large and small classes. The seed weights for large and small seeds were 2.85 ± 0.18 (SD) and 1.74 ± 0.14 (SD) mg/seed, respectively. Cleaned and classified seeds were then sealed in plastic bags and stored at −18 °C until use. Please see Wang et al. (*4*) for details regarding characteristics, location, and year of tested winterfat seeds.

Synchrotron IR Window Preparation. The seed samples were cut into thin cross-sections (ca. 6 μm thick) using a microtome at the University of Saskatchewan. The unstained cross-sections were mounted onto BaF_2 windows (size, 13 mm × 1 mm disk; part no. 915-3015, Spectral Systems, NY) for transmission mode in SR-FTIR microspectroscopic work. More detailed methodology on slide preparation was reported by Yu et al. (*20*).

Photomicrograph of Cross-Sections of Winterfat Seed Tissues. Photomicrographs of cross-sections of the winterfat seed tissues (thickness, 6 μm) were taken with a digital camera from the windows by the S-FTIR microspectroscopy. The magnification is 10×.

Synchrotron Light Source and FTIR Microspectroscopy. This experiment was performed at the National Synchrotron Light Source in Brookhaven National Laboratory (NSLS-BNL, New York). The beamline U10B was equipped with a FTIR spectrometer (Nicolet Magna 860) with a KBr beam splitter and liquid nitrogen-cooled MCT (mercury−cadmium−telluride) detectors coupled with a Continuum IR microscope (Spectra Tech, Shelton, CT) with Schwartzshild 32× objective and 10× condenser. Synchrotron radiation from the VUV storage ring at beamline U10B (with an energy level 800 MeV) entered the interferometer via a port of the instrument designed for use for infrared emission. The IR spectra were collected in the mid-IR range 4000−800 cm^{-1} at a resolution of 4 cm^{-1} with 64 scans coadded. The aperture setting was 10 μm × 10 μm. Stage control, spectrum data collection, and processing were performed using OMNIC 6.0 (Spectra Tech). Scanned visible images were obtained using a charge-coupled device (CCD) camera linked to the infrared images.

Experimental Design, Data Analysis, and Chemical Images. The spectral data of the seed tissues−cotyledons were collected, corrected with the background (no tissue sample) spectrum, displayed in the absorbance mode, and analyzed using OMNIC 6.0 (Spectra Tech). The data were displayed either as a series of spectroscopic images collected at individual wavelengths (such as protein amide I at ca. 1650 cm^{-1}) or as a collection of infrared spectra obtained at each pixel position in the image. Chemical functional groups were identified according to published reports (*13*, *21*−*23*). Chemical imaging of protein (amide I) in the intrinsic structures of the seed tissues was determined by the OMNIC 6.0 software at the spectral region (1650−1550 cm^{-1}) of greatest interest. The protein mapping provided spectra data selected with relatively "pure" protein for modeling amide I component peaks. The selection procedure followed the methodology published by Wetzel et al. (*24*).

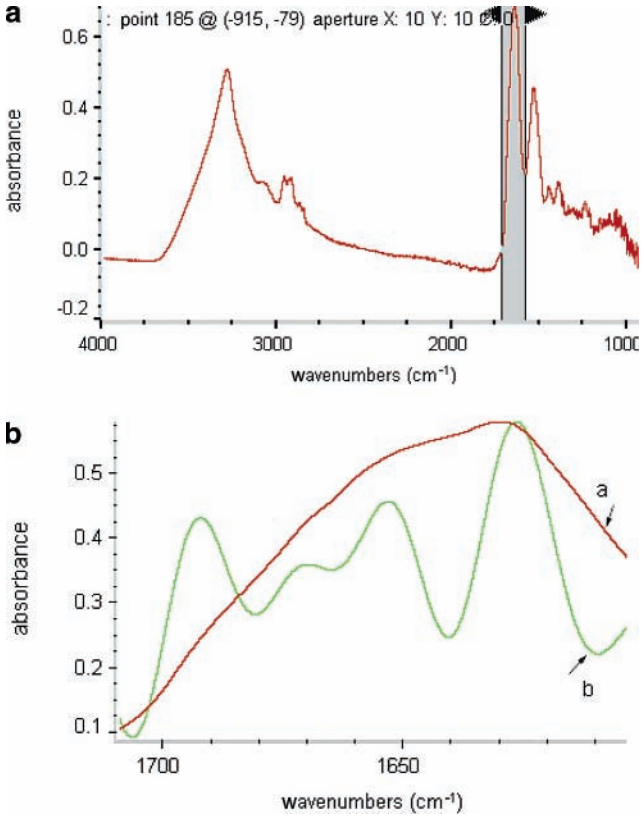

Figure 1. Typical synchrotron FTIR spectrum and Fourier self-deconvolution (FSD) spectrum of winterfat seed tissue (pixel size, 10 μm × 10 μm). (**a**) Amide I band region. (**b**) FSD spectrum of amide I [band center (left to right) at ca. 1690, 1670, 1650, and 1630 cm^{-1}] (**a** = original spectrum; **b** = FSD spectrum).

To get rid of the carbohydrate scattering effect to protein spectrum, the relatively "pure" protein areas in the seed tissues were selected for protein secondary structure analysis. The selected spectrum had very high protein amide I and amide II peaks and no or very little carbohydrate. For large type seeds, 26 relatively "pure" areas were analyzed. For small type seeds, 29 relatively "pure" areas were analyzed. The size of each probed area was 10 μm × 10 μm.

Quantify the Percentage of α-Helix and β-Sheet in Protein Secondary Structures. Because protein amide I component bands were overlapped (**Figure 1**), a specific multipeak fitting or modeling procedure was required. To determine the relative amount of protein secondary structures, two steps were applied. The first step used Fourier self-deconvolution (FSD) in OMNIC to obtain a FSD amide I spectrum in protein amide I region to identify protein amide I component peak frequencies (**Figure 1**). The detailed concepts and algorithm of FSD (FSD, a method for resolving intrinsically overlapped bands) were described in Kauppinen et al. (*25*) and Griffths and Pariente (*26*). The second step used multipeak fitting programs with both Gaussian and Lorentzian functions in Origin V6.1 software (OriginLab Corporation, Northampton, MA) (**Figure 2**) to quantify the multicomponent peak areas in protein amide I bands. The assignment of each component to a particular secondary structure was on the basis of its center frequency according to the following criteria: band center at ca. 1630 cm^{-1}, β-sheet; band center at ca. 1650 cm^{-1}, α-helix; band center at ca. 1670 cm^{-1}, antiparallel β-sheet; and band center at ca. 1690 cm^{-1}, β-turns. It was noticed that protein amide I band frequencies could be affected by other effects, such as amino acid compositions; however, the amide I FSD spectrum band pattern for the winterfat seed (**Figure 1**) was always kept the same and was easily identified. The detailed descriptions have been reported in Origin in terms of peak shape, peak center, offset, wide, and areas. The relative amount of protein secondary structures based on modeled peak area was calculated according to the report generated by the software (**Figure 2**). For example, the percentage of β-sheet was calculated as: % β-sheet = 100 × A1/(A1 + A2 + A3 +

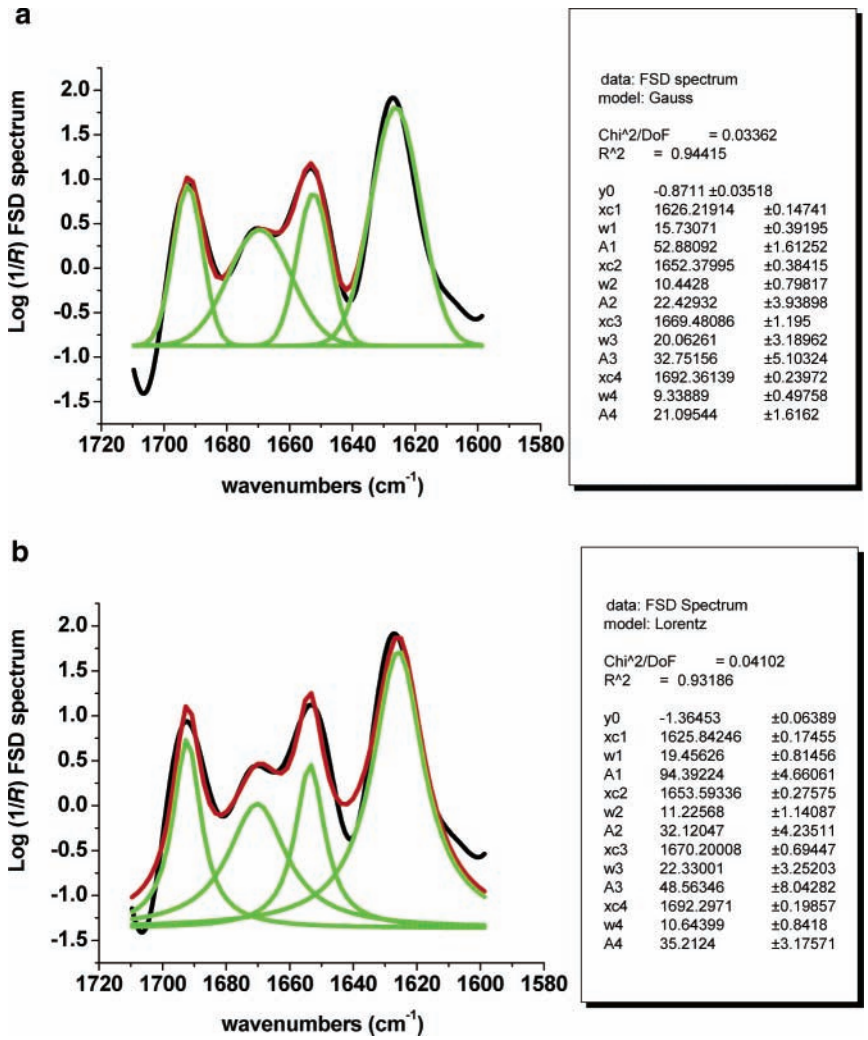

Figure 2. Multicomponent peaks (center at ca. 1690, 1670, 1650, and 1630 cm^{-1}) modeling of typical FSD spectrum of protein amide I in winterfat tissue (Methods of multicomponent modeling: step 1, using Fourier self-deconvolution to obtain FSD amide I spectrum; and step 2, using multipeaks fitting program to quantify the multicomponent peaks area in protein amide I region). (**a**) Multipeaks fitting using Gaussian method showing 16% of ca. 1690, 25% at ca. 1670, 17% of ca. 1650, and 41% at ca. 1630 cm^{-1}. (**b**) Multipeaks fitting using Lorentzian method showing 17% of ca. 1690, 23% at ca. 1670, 16% of ca. 1650, and 45% at ca. 1630 cm^{-1}.

A4); the percentage of α-helix was calculated as: % α-helix = 100 × A2/(A1 + A2 + A3 + A4). The ratio of α-helix to β-sheet was calculated as: ratio = % α-helix/% β-sheet.

Statistical Analysis. Statistical analyses were performed using Proc Mixed of SAS (*27*) with the model: Y = mean + seeds + fitting methods + seed × fitting method + error (where Y = protein secondary structures; seed = large, small; multipeak fitting methods = Gaussian, Lorentzian functions). Significance was declared at $P < 0.05$.

RESULTS AND DISCUSSION

Photomicrograph of Winterfat Seed Tissues. The photomicrographs of cross-sections of the winterfat of the large (L) and small (S) type seeds tissues are presented in **Figure 3**. These photomicrographs only show some of the structural information but do not show the structural−chemical information and do not give any information on localized structural−chemical characteristics. Furthermore, with traditional "wet" chemical analytical methods, it is not possible to determine chemical features of the inherent structures of the winterfat at ultraspatial resolution (3−10 μm) (*13*, *17*−*19*).

Ultra-Spatially Resolved Chemical Mapping of Protein in Winterfat Seeds. Each biological component has an unique molecular chemical−structural feature, and each has its own unique IR spectrum. The characteristic of protein structure is unique in the peptide bond. The peptide bond contains C═O, C−N, and N−H. The amide I bond is primarily a C═O stretching vibration (80%) plus a C−N stretching vibration. Amide I absorbs at ca. 1650 cm^{-1}. Amide II, which absorbs at 1550 cm^{-1}, consists of N−H bending vibrations (60%) coupled with C−N stretching vibrations (40%) (*13*, *15*, *16*, *23*). Carbohydrates contain lots of sugars and lot of OH and CO bonds. Depending on bond linkage and type of sugar, the IR position for carbohydrate is between 1180 and 950 cm^{-1}.[28] For example, starch absorbs at ca. 1025 and 1050 cm^{-1} (*13*, *24*, *29*). **Figure 4** represents color maps of protein of the cotyledon tissue of winterfat seeds and single pixel spectra measuring an area as small as 10 μm × 10 μm of the sample. These maps show the distribution and relative concentration of the protein associated with the seed inherent microstructure, imaged in false color representation of chemical intensities. Blue stands for high, red stands for low intensity, and white stands for no functional groups. The spectrum in the figure corresponds to the pixel in the cross-hair and was selected to represent the value of the integrated peak. **Figure 4** shows the areas under the 1650 cm^{-1} peak attributed to protein amide I absorption (*13*, *23*, *30*), which is an indicator of the area of the sample where protein is present.

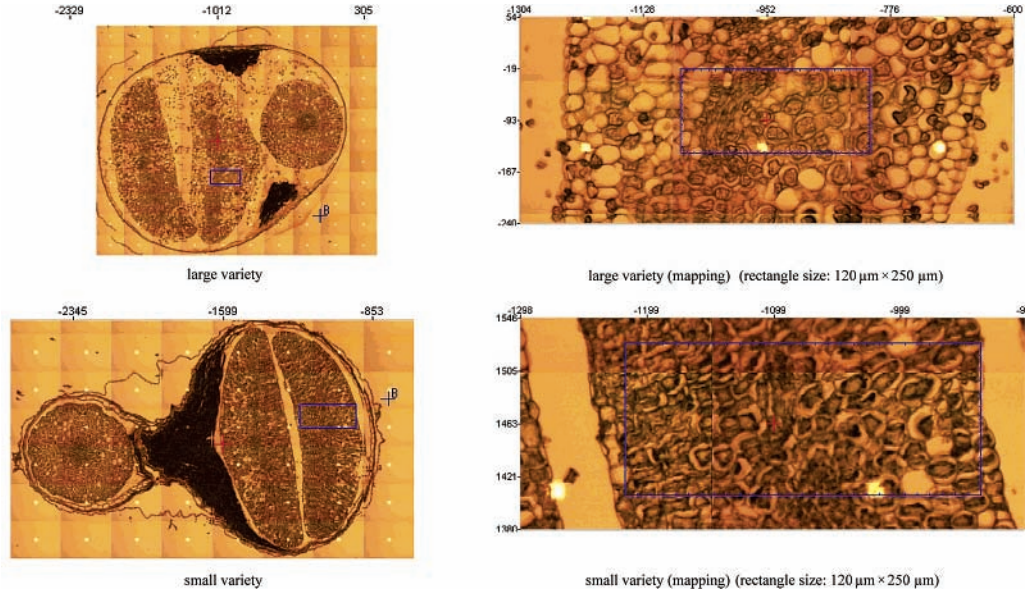

Figure 3. Photomicrograph of cross-section of the large and small varieties of winterfat seed tissues (rectangular areas are cotyledon tissue). Note that the photomicrograph number units are in micrometers (magnification, 10 × 10).

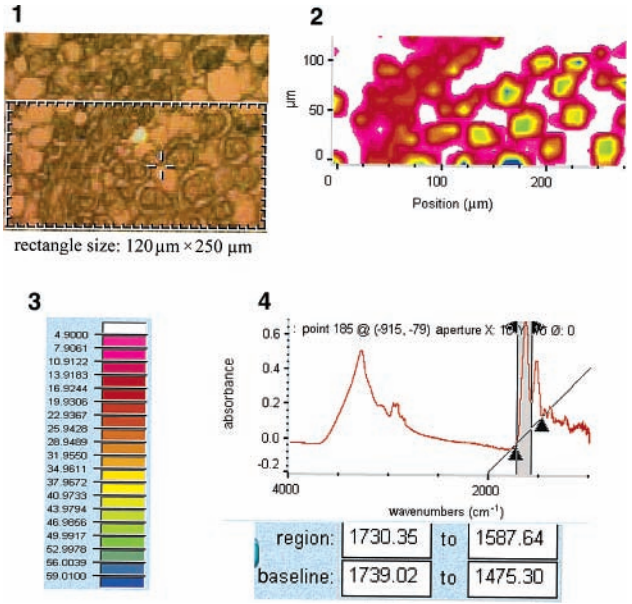

Figure 4. Ultrastructural chemical (functional group) images of the winterfat seed cotyledon tissue. (Large): protein image, area under 1650 cm^{-1} peak area showing protein amide I intensity and distribution, indicating chemical heterogeneous (1, visible image; 2, chemical image; 3, chemical intensity; and 4, spectra corresponding to the pixel at the cross-hair in the visible image) (rectangle size, 120 μm × 250 μm).

Figure 4 clearly shows that protein is unequally distributed in the cotyledon areas of winterfat tissue, indicating heterogeneity of the winterfat cotyledon tissue. Our chemical mapping results demonstrate the potential of highly spatially resolved infrared microspectroscopy to reveal winterfat seed tissue within cellular dimensions. The protein distribution and intensity, even within cellular dimensions in winterfat seed tissue, are unequally distributed, which justify a need to select area with relative "pure" protein for the study of protein secondary structures with minimum disturbance by other biological components such as carbohydrates. If the study is to relatively quantify biological components, ratio maps (such as protein-to-starch ratio) are used in order to get rid of the thickness effect within a tissue.

Table 1. R^2 and χ^2 of Multicomponent Peaks Modeling of FSD Spectrum of Amide I in Winterfat Seed Tissues: Comparison of Large (L) and Small (S) Size Types of Winterfat Seeds[a]

items	modeling method	sample no.	modeling R^2 (±SD)	modeling χ^2 (±SD)
L	Gauss	26	0.99 (±0.01) a	0.00499 (±0.00511) b
	Lorentz	26	0.97 (±0.02) b	0.01631 (±0.01448) a
S	Gauss	29	0.99 (±0.01) a	0.00518 (±0.00614) b
	Lorentz	29	0.97 (±0.01) b	0.01723 (±0.10757) a
SEM			0.008	0.001871
			seed mean	
L		52	0.98	0.01065
S		58	0.98	0.01120
SEM			0.002	0.00132

[a] Means with the same letter in the same column are not significantly different ($P > 0.05$). SEM, standard error of mean.

Characteristics of Protein Secondary Structures of Winterfat Seed Tissue Indicated by Amide I Infrared Band. Typical, protein secondary structures mainly include the α-helix and β-sheet (*31*, *32*). The protein IR spectrum has two primary features, as indicated before, the amide I (ca. 1600−1700 cm^{-1}) and amide II (ca. 1500−1560 cm^{-1}) bands, which arise from specific stretching and bending vibrations of the protein backbone. The vibrational frequency of the amide I band is particularly sensitive to protein secondary structure (*21*, *24*, *33*, *34*) and can be used to predict protein secondary structure. For α-helix, the amide I is typically in the range of 1648−1658 cm^{-1}. For the β-sheet, the peak can be found within the range of 1620−1640 cm^{-1} (*33*). The amide II (predominantly an N−H bending vibration coupled to C−N stretching) is also used to assess protein conformation. However, as it arises from complex vibrations involving multiple functional groups, they are less useful for protein structure prediction than the amide I band (*23*). **Figure 1** shows typical protein amide I and amide II spectra of the winterfat seed tissues. The spectrum of amide I original band shows peaks at ca. 1690, 1670, 1650, and 1630 cm^{-1} (**Figure 1**). This was confirmed from a FSD spectrum of amide I in **Figure 1**.

Modeling of Protein Amide I Peaks To Quantify the Percentage of Protein Secondary Structures. Because of

Table 2. Percentage of FSD Amide I Peaks at 1650, 1630, 1670, and 1690 cm^{-1} of Winterfat Seed Tissues: Comparison of Large (L) and Small (S) Size Types of Winterfat Seeds, Indicating the Characteristics of Protein Secondary Structures[a]

			% of peak at			
items	modeling method	sample no.	1650 cm^{-1} (±SD)	1630 cm^{-1} (±SD)	1670 cm^{-1} (±SD)	1690 cm^{-1} (±SD)
L	Gauss	26	26.00 (±7.58) a	36.77 (±6.92)	20.19 (±4.23) ab	17.04 (±3.18) c
	Lorentz	26	23.68 (±8.03) ab	38.72 (±7.69)	18.36 (±3.72) b	19.24 (±3.50) b
S	Gauss	29	24.98 (±6.15) ab	36.12 (±3.66)	20.96 (±5.58) a	17.94 (±2.08) bc
	Lorentz	29	21.67 (±5.66) b	36.26 (±3.68)	19.87 (±5.31) ab	22.20 (±2.51) a
SEM			1.312	1.086	0.919	0.543
			seed mean			
L		52	24.84	37.74	19.28	18.14 a
S		58	23.32	36.19	20.42	20.07 b
SEM			0.928	0.768	0.650	0.384

[a] Means with the same letter in the same column are not significantly different ($P > 0.05$) (LSD test). SEM, standard error of mean.

Table 3. Ratios of Protein Amide I FSD Peaks of Winterfat Seed Tissues: Comparison of Large (L) and Small (S) Size Types of Winterfat Seeds, Indicating the Characteristics of Protein Secondary Structures

Section a[a]

items	modeling method	sample no.	ratio of 1650 to 1630 cm^{-1} (±SD)	ratio of 1650 to 1670 cm^{-1} (±SD)
L	Gauss	26	0.77 (±0.38) a	1.40 (±0.68)
	Lorentz	26	0.67 (±0.38) ab	1.40 (±0.77)
S	Gauss	29	0.70 (±0.21) ab	1.37 (±0.76)
	Lorentz	29	0.60 (±0.18) b	1.26 (±0.79)
SEM			0.057	0.144
		seed mean		
L		52	0.72	1.40
S		58	0.65	1.32
SEM			0.040	0.102

Section b[b]

items	modeling method	sample no.	ratio of 1650 to 1690 cm^{-1} (±SD)	ratio of 1630 to 1670 cm^{-1} (±SD)	ratio of 1690 to 1630 cm^{-1} (±SD)
L	Gauss	26	1.58 (±0.60) a	1.88 (±0.45)	0.49 (±0.17) b
	Lorentz	26	1.30 (±0.60) b	2.18 (±0.52)	0.53 (±0.17) b
S	Gauss	29	1.42 (±0.42) ab	1.87 (±0.62)	0.50 (±0.09) b
	Lorentz	29	1.00 (±0.31) c	2.00 (±0.72)	0.62 (±0.11) a
SEM			0.094	0.113	0.0263
			seed mean		
L		52	1.44 a	2.03	0.51 b
S		58	1.21 b	1.93	0.56 a
SEM			0.067	0.080	0.019

[a] Means with the same letter in the same column are not significantly different ($P > 0.05$). SEM, standard error of mean. [b] Means with the same letter in the same column are not significantly different ($P > 0.05$) (LSD test). SEM, standard error of mean.

protein amide I component peaks overlapping within each other (**Figure 1**), FSD was used to obtain the FSD amide I spectrum to identify amide I component peak frequencies (**Figure 2**), and then, multicomponent peak fittings with Gaussian and Lorentzian functions were used to quantify the multicomponent peak area in the protein amide I region.

Table 1 shows R^2 and χ^2 of multicomponent peaks modeling of the FSD spectrum of amide I in the winterfat seed tissues. No differences were found between the two types of seed tissues. However, in terms of modeling methods, the Gaussian method is better than the Lorentzian method with higher R^2 and lower χ^2. **Tables 2** and **3** show percentages and ratios of protein secondary structures of the winterfat tissues. As compared to the two types of the winterfat seeds, the large type of seeds contained no significant differences ($P > 0.05$) in percentage of β-sheet (average 37.0%) and α-helix (average 24.1%). However, the large seed type contained a lower ($P < 0.05$) percentage of β-turns (18.1 vs 20.1%) (**Table 2**) but no difference in percentage of α-helices and β-sheets and higher ($P < 0.05$) ratios of α-helices to β-turns (1.4 vs 1.2) and lower ($P < 0.05$) ratios of β-turns to β-sheets (0.5 vs 0.6) (**Table 3**). These results indicated that (i) the large and small types of winterfat seeds have subtly different protein secondary structure profiles, which implicate differences in structural−chemical makeup and features of the two types of winterfat seeds. These subtle differences may affect seed quality and growth characteristics (*4*). Keeping in mind current research on "prion diseases", perhaps only subtle changes in secondary structure are needed to provide big consequences. It is needed to mention that our results should be considered as typical and not average for the individual winterfat seeds, because many factors will affect the quality of seeds, such as location, climate, and growth conditions. Information from this study by the infrared probing protein secondary structure may be valuable as a guide for winterfat breeders to improve and maintain seed quality. Our results demonstrate the potential of highly spatially resolved

synchrotron-based FTIR microspectroscopy to localize chemical microstructure and reveal protein secondary structure of the winterfat seeds at a cellular level, which may provide an indication of the quality of seed storage protein affecting seed germination characteristics. Large seeds of winterfat germinated significantly faster and higher in germination percentage than small seeds at low and subzero temperatures (*11*). Higher cold resistance in large seeds was correlated with seed composition, such as the higher contents of glucose, raffinose, and sucrose during germination. The difference of chemical feature in protein secondary structure between large and small seeds may also be associated with the higher cold tolerance of large seeds. The irreversible change in protein secondary structures was associated with seed tolerance to desiccation in *Quercus alba* L. (*12*). The levels of α-helix and β-sheet secondary structure fractions were relatively conservative in seed globulins between monocotyledonous and dicotyledonous crops (*35*). The protein secondary structure variation between seed size in winterfat seeds showed the high variation in a natural population, which may be related to the natural adaptation in this native species. However, there is an equally plausible hypothesis untested in this area that "large" seeds may be softer and germinate faster and/or possess all sorts of admirable postgermination properties merely because of the polysaccharide composition/structure of the outer seed coat(s). This area is needed to investigate further.

In conclusion, with synchrotron-based FTIR microspectroscopy, the molecular structrual−chemical makeup characteristics could be imaged and revealed at a high ultraspatial resolution (10 μm). Synchrotron-based FTIR microspectroscopy revealed that the secondary structures of protein differed between the large and the small winterfat seeds in mid-IR within cellular dimensions. By using multicomponent peaks modeling, the results show that the large types of seeds contained no significant differences in percentages of β-sheets (average 37.0%) and α-helices (average 24.1%). However, the large seed type contained lower ($P < 0.05$) percentages of β-turns (18.1 vs 20.1%) (**Table 2**) and but no difference in percentages of α-helices and β-sheets and higher ($P < 0.05$) ratios of α-helices to β-turns (1.4 vs 1.2) and lower ($P < 0.05$) ratios of β-turns to β-sheets (0.5 vs 0.6). These results indicated microstructural−chemical differences of protein secondary structures between the large and the small winterfat seeds, and the variation may affect seed germination behaviors during early seedling development. Further study is needed to systematically quantify the relationship between protein secondary structures and seed germination characteristics and stress tolerance in winterfat.

ACKNOWLEDGMENT

We are grateful to Drs. Lisa Miller and Wang Qi (NSLS-BNL, New York) for helpful data collection at U10B Experimental Station.

LITERATURE CITED

(1) Call, C. A.; Roundy, B. A. Perspectives and processes in revegetation of arid and semiarid rangelands. *J. Range Manage.* **1991**, *44*, 543−549.

(2) Romo, J. T.; Redmann, R. E.; Kowalenko, B. L.; Nicholson, A. R. Growth of winterfat fowling defoliation in Northern Mixed Prairie of Saskatchewan. *J. Range Manage.* **1995**, *48*, 240−245.

(3) Hou, J. Q.; Romo, J. T. Seed weight and germination time affect growth of 2 shrubs. *J. Range Manage.* **1998**, *51*, 699−703.

(4) Wang, R.; Bai, Y.; Tanino, K. Effect of seed size and sub-zero imbibition temperature on the thermal time model of winterfat (*Eurotia lantata* (Pursh) Mog.). *Environ. Exp. Bot.* **2004**, *51*, 183−197.

(5) Lafound, G. P.; Baker, R. J. Effects of temperature, moisture stress and seed size on germination of nine spring wheat cultivars. *Crop Sci.* **1986**, *26*, 563−567.

(6) Berdahl, J. D.; Frank, A. B. Seed maturity in four cool-season forage grasses. *Agron. J.* **1998**, *90*, 483−488.

(7) Dalling, J. W.; Hubbell, S. P. Seed size, growth rate and gap microsite conditions as determinants of recruitment success for pioneer species. *J. Ecol*. **2002**, *90*, 557−568.

(8) Debain, S.; Curt, T.; Lepart, J. Seed mass, seed dispersal capacity, and seedling performance in a Pinus sylvestris population. *Ecoscience* **2003**, *10*, 168−175.

(9) Simons, A. M.; Johnston, M. O. Variation in seed traits of *Lobelia inflata* (*Campanulaceae*): Sources and fitness consequences. *Am. J. Bot.* **2000**, *87*, 124−132.

(10) Walters, M. B.; Reich, P. B. Seed size, nitrogen supply, and growth rate affect tree seedling survival in deep shade. *Ecology* **2000**, *81*, 1887−1901.

(11) Wang, R.; Bai, Y.; Low, N. H.; Tanino, K. Seed size variation in cold and freezing tolerance during seed germination of winterfat (*Krascheninnikovia lanata*) (Chenopodiaceae). *Can. J. Bot.* **2005**, in press.

(12) Connor, K. F.; Sowa, S. Effects of desiccation on the physiology and biochemistry of *Quercus alba* acorns. *Tree Physiol.* **2003**, *23*, 1147−1152.

(13) Wetzel, D. L.; Eilert, A. J.; Pietrzak, L. N.; Miller, S. S.; Sweat, J. A. Ultraspatially resolved synchrotron infrared microspectroscopy of plant tissue in situ. *Cell. Mol. Biol.* **1998**, *44*, 145−167.

(14) Holman, H.-Y. N.; Bjornstad, K. A.; McNamara, M. P.; Martin, M. C.; McKinney, W. R.; Blakely, E. A. Synchrotron infrared spectromicroscopy as a novel bioanalytical microprobe for individual living cells: Cytotoxicity considerations. *J. Biomed. Opt.* **2002**, *7*, 1−10.

(15) Miller, L. M. The impact of infrared synchrotron radiation on biology: Past, present, and future. *Synchrotron Radiat. News* **2000**, *13*, 31−37.

(16) Marinkovic, N. S.; Huang, R.; Bromberg, P.; Sullivan, M.; Toomey, J.; Miller, L. M.; Sperber, E.; Moshe, S.; Jones, K. W.; Chouparova, E.; Lappi, S.; Franzen, S.; Chance, M. R. Center for Synchrotron Biosciences' U2B beamline: An international resource for biological infrared spectroscopy. *J. Synchrotron Radiat.* **2002**, *9*, 189−197.

(17) Budevska, B. O. In *Handbook of Vibrational Spectroscopy, Vol. 5. Applications of Vibrational Spectroscopy in Life, Pharmaceutical and Natural Sciences*; Chalmers, J. M., Griffiths, P. R., Eds.; John Wiley and Sons: New York, 2002; pp 3720−3732.

(18) Wetzel, D. L. When molecular causes of wheat quality are known, molecular methods will supersede traditional methods. Proceedings of the International Wheat Quality Conference II, Manhattan, Kansas, May 2001; pp 1−20.

(19) Yu, P. Application of advanced synchrotron-based Fourier transform infrared microspectroscopy (SR-FTIR) to animal nutrition and feed science: a novel approach. *Br. J. Nutr.* **2004**, *92*, 869−885.

(20) Yu, P.; McKinnon, J. J.; Christensen, C. R.; Christensen, D. A.; Marinkovic, N. S.; Miller, L. M. Chemical imaging of microstructures of plant tissues within cellular dimension using synchrotron infrared microspectroscopy. *J. Agric. Food Chem.* **2003**, *51*, 6062−6067.

(21) Kemp, W. *Organic Spectroscopy*, 3rd ed.; W. H. Freeman and Company: New York, 1991.

(22) Himmelsbach, D. S.; Khalili, S.; Akin, D. E. FT-IR microspectroscopic imaging of flax (linum usitatissimum L.) stems. *Cell. Mol. Biol.* **1998**, *44*, 99−108.

(23) Jackson, M.; Mantsch, H. H. Infrared spectroscopy ex vivo tissue analysis. In *Encyclopedia of Analytical Chemistry*; Meyers, R. A., Ed.; John Wiley and Sons Ltd.: Chicherster, 2000; pp 131−156.

(24) Wetzel, D. L.; Srivarin, P.; Finney, J. R. Revealing protein infrared spectral detail in a heterogeneous matrix dominated by starch. *Vib. Spectrosc.* **2003**, *31*, 109−114.

(25) Kauppinen, J. K.; Moffatt, D. J.; Mantsch, H. H.; Cameron, D. G. Fourier selfdeconvolution: A method for resolving intrinsically overlapped bands. *Appl. Spectrosc*. **1981**, *35*, 271−276.
(26) Griffths, P. R.; Pariente, G. Trends in analytical chemistry. *Introduction to Spectral Deconvolution*; 1986; Vol. 5, p 209.
(27) SAS. *User's Guide: Statistics*, 8th ed.; SAS Inst., Inc.: Cary, NC, 1998.
(28) Yu, P.; McKinnon, J. J.; Christensen, C. R.; Christensen, D. A. Using synchrotron transmission FTIR microspectroscopy as a rapid, direct and nondestructive analytical technique to reveal molecular microstructural-chemical features within tissue in grain barley. *J. Agric. Food Chem.* **2004**, *52*, 1484−1494.
(29) Yu, P.; McKinnon, J. J.; Christensen, C. R.; Christensen, D. A. Imaging molecular chemistry of Pioneer corn. *J. Agric. Food Chem*. **2004**, *52*, 7345−7352.
(30) Yu, P.; Christensen, D. A.; Christensen, C. R.; Drew, M. D.; Rossnagel, B. G.; McKinnon, J. J. Use of synchrotron FTIR microspectroscopy to identify chemical differences in barley endosperm tissue in relation to rumen degradation characteristics. *Can. J. Anim. Sci.* **2004**, *84*, 523−527.
(31) Dyson, H. J.; Wright, P. E. Peptide conformation and protein folding. *Curr. Opin. Struct. Biol.* **1990**, *3*, 60−65.
(32) Carey, F. A. *Organic Chemistry*, 3rd ed.; McGraw-Hill Companies, Inc.: New York, 1996.
(33) Martin, M. C. Fourier-tranform infrared spectroscopy. Retrieved in October 2002 from http://infrared.als.lbl.gov/.
(34) Seguchi, M.; Takemoto, M.; Mizutani, U.; Ozawa, M.; Nakamura, C.; Matsumura, Y. Effects of secondary structures of heated egg white protein on the binding between prime starch and tailings fractions in fresh wheat flour. *Cereal Chem.* **2004**, *81*, 633−636.
(35) Marcone, M. F.; Kakuda, Y.; Yada, R. Y. Salt-soluble seed globulins of dicotyledonous and monocotyledonous plants. II. Structural characterization. *Food Chem*. **1998**, *63*, 265−274.

Received for review July 20, 2005. Revised manuscript received October 6, 2005. Accepted October 8, 2005. This research has been supported by grants from the Natural Sciences and Engineering Research Council of Canada [NSERC-Individual Discovery Grant (P.Y.)] and Saskatchewan Agricultural Development Fund (ADF). The National Synchrotron Light Source in Brookhaven National Laboratory (NSLS-BNL, New York) is supported by U.S. Department of Energy Contract DE-AC02-98-CH10886.

JF051748+